PAPER

Check for updates

Double cross-linked cellulose hydrogel-supported Fe species for efficient wound healing

Mingyue Xue,[a] Xianglin Pei, [ID] *[a] Jian Zhang,[b] Cuiling Niu,[d] Hongqin Wang,[a] Ling Nie*[c] and Jiuyang Ding*[b]

Traditional dressings often lack adequate skin structure support, which can lead to secondary damage, poor hemostasis, and an increased risk of inflammation due to wound adhesion. In this work, cellulose hydrogels were prepared by physical/chemical double cross-linking *via* a 'sol–gel' strategy and further loaded with Fe to obtain a three-dimensional (3D) porous cellulose/Fe composite hydrogel (cellulose/Fe gel). The obtained cellulose/Fe gel featured a 3D porous nanofiber structure, excellent water absorption/moisture retention performance, and good mechanical stability. Moreover, it could effectively remove reactive oxygen species (ROS) and inhibit cellular oxidative stress, demonstrating potential anti-inflammatory effects. When applied to wound repair in rats, cellulose/Fe gel, with excellent cell compatibility, effectively stimulated the formation of new blood vessels and significantly reduced the level of inflammatory factors, promoting wound healing. This work provides a new approach for cellulose-based hydrogel wound dressings.

1. Introduction

The skin is the primary defense barrier of the human body and is vulnerable to various types of damage, including mechanical damage, burns, scalds, and iatrogenic injuries. Among these, mechanical damage is the most common. The process of skin wound healing is typically divided into four continuous and possibly overlapping stages: hemostasis, inflammation, proliferation, and remodeling. These processes are affected by a complex network of multiple cells and biological media[1] and are often accompanied by bacterial invasion or vascular damage. Such complications can lead to infection, bleeding, and even disability or death, making wound treatment a challenging task in clinical practice.[2–5] Traditional wound gauze dressings used in clinical settings help to dry the wound by absorbing exudates, but they can easily adhere to the wound, causing difficulty in separation and leading to secondary damage during dressing removal.[6] Moreover, traditional wound gauze dressings generally lack antibacterial and anti-inflammatory properties and thus cannot effectively promote wound healing. Therefore, there is a significant need for the development of new dressings that can fully protect the wound,

maintain an appropriate moist environment, and offer biodegradability, anti-inflammatory and homeostatic properties.[7–9]

Recently, natural polymers with low cost, high biological activity, excellent biocompatibility and good biodegradability have been extensively developed for hemostasis and wound healing.[10–13] In particular, natural polymer-based hydrogels, in addition to these advantages, offer strong water absorption, good stability and a 3D porous structure resembling the extracellular matrix (ECM), providing a unique advantage in wound repair.[14] Compared with traditional commercial wound dressings, natural polymer-based hydrogel dressings offer the following advantages: (1) maintaining a moist environment at the wound site, reducing pain; (2) good modeling ability and mechanical properties to meet the requirements of complex wound healing (*e.g.*, burns, chronic ulcers, and damaged tissues); (3) excellent light transmittance and high porosity, which accelerate the penetration of nutrients and oxygen, thereby accelerating wound healing;[15] (4) the ability to effectively inhibit bacterial infection,[16] promote the formation of granulation tissue and re-epithelialization, and reduce the formation of scars.

In this work, we used cellulose, the most abundant natural polymer, and dissolved it in a low-temperature alkali/urea aqueous system to obtain a regenerated cellulose solution, followed by cross-linking with a cross-linking agent to prepare a physicochemical double-crosslinked cellulose hydrogel through a 'sol–gel' strategy.[17] The cellulose hydrogel obtained by the above method has good stability and a clear moisturizing effect, and may be used for complex wounds to effectively avoid secondary damage during wound healing. At the same time, its loose 3D porous structure is conducive to the transport of nutrients and oxygen to the cells attached to the gel, promoting

[a]School of Materials and Architectural Engineering, Guizhou Normal University, Guiyang, 550025, China. E-mail: xianglinpei@163.com

[b]School of Forensic Medicine, Guizhou Medical University, Guiyang, 550004, China. E-mail: djy09099@163.com

[c]School of Materials Science & Engineering, Hubei University of Automotive Technology, Shiyan, 442002, China. E-mail: nieling2023@126.com

[d]Yunnan Characteristic Plant Extraction Laboratory, College of Chemical Science and Technology, Yunnan University, Kunming, 650091, China

the wound healing process. Furthermore, we incorporated Fe into the cellulose hydrogel to prepare a cellulose/Fe composite hydrogel, based on the following consideration: (1) Fe can further induce the crosslinking of cellulose and enhance the mechanical properties of the cellulose hydrogels; (2) due to the flocculation of Fe^{3+}, it can neutralize the negative charge of blood cells to make colloidal particles aggregate, and it plays a role in stabilizing and accelerating coagulation;[18] (3) Fe^{3+} is also an inorganic catalyst that can effectively promote the decomposition of H_2O_2 to generate oxygen.[19] Moreover, studies have shown that in some cases, Fe^{3+} can promote the activity of some antioxidant enzymes, thereby indirectly exerting antioxidant effects. Fe ions can also react with free radicals to form stable complexes, reducing cell damage from free radicals.[20,21] At the same time, Fe ions can exert anti-inflammatory effects through multiple pathways to promote wound repair. For example, it can inhibit the production of pro-inflammatory factors such as TNF-α and IL-1β.[22,23] The cytotoxicity of the cellulose/Fe hydrogel was evaluated by *in vitro* culture of human dermal fibroblasts cells and flow cytometry, and the ability of the cellulose/Fe hydrogel to accelerate wound recovery was assessed by a Sprague–Dawley (SD) rat wound model. The results showed that the cellulose/Fe hydrogel facilitated cell viability and proliferation *in vitro*, accelerated angiogenesis *in vivo*, and promoted granulation tissue formation and collagen deposition, resulting in fast would healing. This work uses low-cost and sustainable biomass resources as raw materials to construct cellulose-loaded Fe wound dressings, which provides new opportunities for their wide application in the clinical field.

2. Experimental section

2.1 Materials

Cellulose cotton linter pulp (α-cellulose content higher than 95%) was provided by the Hubei Chemical Fiber Group Co., Ltd (Xiangfan, China). LiOH·H_2O (98%) and urea (99%) were purchased from Sinopharm Chemical Reagents Co., Ltd (Shanghai, China). $Fe(NO_3)_3 \cdot 9H_2O$ (99%) and epichlorohydrin (EPI, 99%) were purchased from China Macklin Reagent Co., Ltd (Shanghai, China). Ethanol (99.9%) was purchased from Chongqing Chuandong Chemical Co., Ltd (China). 3-(4,5-Dimethyl-2-thiazolyl)-2,5-diphenyl tetrazolium bromide (MTT) was purchased from Xi'a Biotech Co., Ltd (China). The LIVE/DEAD™ Baclight™ Bacterial Viability Assay Kit (L7012) was purchased from Invitrogen (China). Rabbit monoclonal anti-CD31 antibody (Cat#ab182981, Abcam, USA), anti-8-hydroxy-2′-deoxyguanosine antibody (Cat#48508, Abcam, USA), anti-TNF-α antibody (Cat#ab1793, Abcam, USA), the SP rabbit & mouse HRP immunohistochemistry DAB kit, mouse IL-1β ELISA kit (Cat#E-MSEL-M0003, Elabscience, China), mouse IL-6 ELISA kit (Cat#E-HSEL-M0003, Elabscience, China) and Masson's trichrome stain kit (Cat#G1340, Solarbio Life Science, China) were used as received without further purified.

2.2 Preparation of cellulose hydrogel

LiOH, urea and H_2O were mixed into a solvent according to a mass ratio of 8 : 15 : 77, and pre-cooled to −15 °C. In the semi-ice and semi-water state, a certain amount of cellulose cotton linter pulp was added and stirred vigorously to obtain a cellulose solution. After centrifugation at 8000 rpm for 5 min, the sediment was evenly distributed onto a glass plate using a casting technique. The processed plate was then immersed in a container filled with ethanol for another 12 h to facilitate the gelation. The cellulose hydrogel, designated as initial cellulose gel, was obtained by repeated washing with deionized water.

For the double cross-linked cellulose hydrogel, a small amount of chemical crosslinking agent epichlorohydrin (EPI) was added dropwise to the above cellulose solution at 0 °C, and stirred for 2 h to obtain a pre-crosslinked cellulose solution. Same as before, after the above cellulose solution was centrifuged (8000 rpm, 5 min), it was attached to the glass plate by casting method and placed in a container of ethanol for 12 h. The cellulose hydrogel was obtained by repeated washing with deionized water, and referred to as cellulose gel.

2.3 Preparation of the cellulose/Fe composite hydrogel

To prepare the cellulose/Fe composite hydrogel, 0.75 g of $Fe(NO_3)_3 \cdot 9H_2O$ was added to deionized water. Then, 5 g of the prepared cellulose hydrogel was added and stirred for 3 h. The hydrogel was then washed repeatedly to remove the residual Fe salt that was not closely combined with cellulose to obtain the cellulose/Fe composite hydrogel, which was referred to as cellulose/Fe gel.

2.4 Materials characterization

The surface and cross-section morphology of the hydrogel samples were observed by field emission scanning electron microscopy (SEM, Zeiss, Germany). Before the test, the hydrogel was freeze-dried and sprayed with gold for 120 s, and the electron acceleration voltage was set to 5 kV. The wide-angle X-ray diffraction (XRD) patterns of the samples were measured using a Miniflex600 diffractometer (Rigaku, Japan) with a scanning angle range of 5°–60° and a scanning speed of $1°$ min^{-1}. Fourier transform infrared spectroscopy (FT-IR) measurements were performed on a Nicolet 5700, SEMAFE, USA. The elemental composition, chemical state and molecular structure of the sample surface were determined by a Kratos XSAM800 photoelectron spectrometer (XPS). The thermogravimetric curves (TG) of the samples were measured using a thermogravimetric analyzer (TA, Q500, USA) over a temperature range of 30 °C–800 °C in a nitrogen atmosphere, with a heating rate of 5 °C min^{-1}. The specific surface area and pore size distribution of the samples were determined by physical adsorption instrument (Autosorb-iQ). The content of the Fe ions was determined by an inductively coupled plasma optical emission spectrometer (ICP-OES). The mechanical properties of cellulose and the composite hydrogels were tested on a universal mechanical testing machine equipped with a pneumatic clamp (Model 5576, INSTRON, USA). The sample size was determined to be 40 mm × 8 mm × 1 mm, and the tensile speed was 1 cm min^{-1}.

2.5 Oxygen generation and monitoring

The oxygen production capacity of the hydrogels was monitored separately in H_2O_2 and phosphate buffered saline (PBS, pH = 7.4, 0.01 M). Typically, $Fe(NO_3)_3 \cdot 9H_2O$ solution (500 μg mL^{-1}), cellulose or/and cellulose/Fe gel (380 mg each) were added to 10 mL of 10 mM H_2O_2 solution. It was then immediately immersed in a dissolved oxygen meter probe (s9-standard Kit, Mettler Toledo, Switzerland), and the oxygen concentration was recorded every 30 s for the next 30 min. As a control, $Fe(NO_3)_3 \cdot 9H_2O$ solution (500 μg mL^{-1}), cellulose gel or cellulose/Fe gel were added to 10 mL PBS at the amount of 380 mg each, and the oxygen concentration was recorded every 30 s according to the above method.[24]

2.6 Cell viability of hydrogels *in vitro*

The cytotoxicity of the hydrogel was observed by MTT assay using human dermal fibroblasts cells (HDF, 4186699, Weibo, China).[25] The cells were inoculated at a density of 6000 cells per well, and the samples were introduced 24 h post-seeding. The blank control group received no treatment, while the experimental groups were treated with a 1.3% $Fe(NO_3)_3 \cdot 9H_2O$ solution, freeze-dried cellulose gel, and cellulose/Fe gel samples. After 48 h of culture, the medium was refreshed, and MTT solution (20 μL) was added and allowed to stand for 4 h. After removing the medium, DMSO (150 μL) was mixed with the substrate. The relative viability of cells was calculated by Multiskan FC (Thermo Fisher), according to the absorbance of the solution at 570 nm. The biocompatibility of the four experimental groups was further evaluated by Annexin V/PI double staining kit.[26] After incubation for a period of time, Annexin V and PI were used for staining for 15 min and 3 min, respectively. The cells were then observed and photographed using a fluorescence microscope (Nikon TS 100, Japan).

2.7 Detection of apoptosis by flow cytometry

RAW264.7 cells, in their logarithmic growth phase, were seeded into 6-well plates. The cells were categorized into four groups under specific conditions: a blank control group, a group treated with an iron salt solution of $Fe(NO_3)_3 \cdot 9H_2O$, a group treated with a cellulose hydrogel, and a group treated with a cellulose/Fe hydrogel. After a 4 h treatment period, the cells were gently washed with pre-cooled 1× PBS and then resuspended in 1× binding buffer (100 μL). A total of 1×10^6 cells were double-stained with Annexin V (5 μL) and PI (5 μL). The volume was adjusted to 500 μL with additional 1× binding buffer. The cells were maintained in the dark and analyzed using flow cytometry within one hour. Quadrant analysis was performed by FCS express v6.0 to calculate the percentage of healthy cells, low apoptotic cells, high apoptotic cells and dead cells. For Annexin V/PI double staining, we follow the manufacturer's instructions and perform flow cytometry analysis under the same condition.

2.8 Rats whole thickness skin wound model

SD rats (male, 180 g–200 g, 6–8 weeks old) were purchased from the Experimental Animal Center of Guizhou Medical University. They were kept in a temperature-controlled room, and fed with standard food and water. Rats were deeply immersed (ketamine 120 mg kg^{-1} and xylazine 8 mg kg^{-1}, *in vitro*). After depilation, a full-thickness skin injury with a diameter of about 10 mm was created on the back of the rat. The rats were randomly divided into four groups: blank control group, 1.3% $Fe(NO_3)_3 \cdot 9H_2O$ solution smearing wound group, cellulose hydrogel treatment group, and cellulose/Fe hydrogel treatment group. The wound size was recorded on days 0, 3, 7 and 14. The wound closure rate was calculated using the following formula (1):

$$\text{Healing rate} = (S_0 - S_t)/S_0 \times 100\% \tag{1}$$

where S_0 represents the original size of the wound area, and S_t represents the wound area recorded on a particular day.[27] All animal experiments were performed according to NIH guidelines, and approved by the Animal Care and Use Committee of Guizhou Medical University.

2.9 Histological and immune histological assessment

On day 14, the wound tissue was collected and soaked in 4% formalin solution for 48 h. After paraffin embedding, tissue sections with a thickness of 3 μm were prepared using a slicing machine (RM 2235, Leica, Germany). Histopathological examination and immunohistochemical analysis were conducted, which included staining with hematoxylin and eosin (H&E) to assess the tissue morphology, Masson trichrome staining to evaluate the collagen content, and immunohistochemical staining for platelet endothelial cell adhesion molecule-1 (CD31), 8-hydroxydeoxyguanosine (8-OHdG), and tumor necrosis factor-α (TNF-α) to assess the specific biological markers. The prepared sections were then imaged and quantitatively analyzed by light microscopy (Nikon A1R/A1, Japan). Image-Pro Plus 6.0 (Media Cybernetics, Inc., Rockville, MD) was used to evaluate the collagen density and the amount of neovascularization in the histological skin samples. In animal experiments, we performed independent experiments on 4 animals ($n = 4$) in each group, and at least 3 biological samples were repeated in each group of H&E, Masson and immunohistochemical staining experiments.

2.10 ELISA analysis and statistical analysis

Enzyme-linked immunosorbent assay (ELISA) was performed using tumor necrosis factor-α (TNF-α), interleukin-6 (IL-6), and interleukin-1β (IL-1β) kits (R & D Systems, Minneapolis, Minnesota). We tested samples in strict accordance with the manufacturer's instructions.

All data were expressed as mean (mean) ± mean standard error (SEM). One-way ANOVA by Bonferroni's *post hoc* analysis was conducted when comparing multiple groups. The p value was set as <0.05.
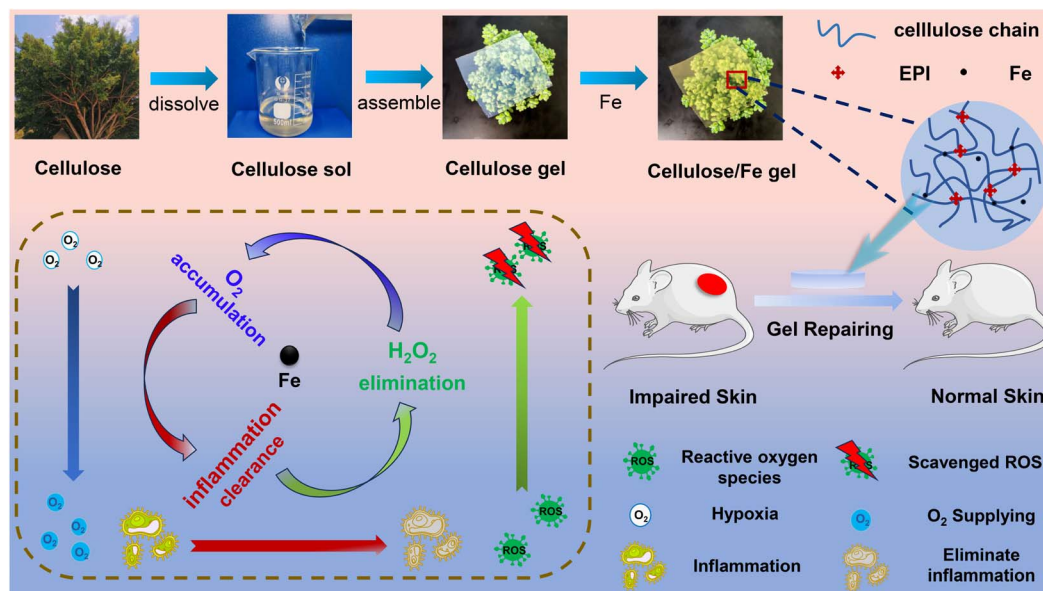
3. Results and discussion

3.1 Preparation and characterization of the cellulose/Fe gel

Scheme 1 illustrates the preparation process of the cellulose/Fe composite hydrogel and its application as a wound dressing.

Scheme 1 Schematic of the preparation of the cellulose/Fe gel and its application as a wound dressing material.

Firstly, the regenerated cellulose solution was obtained by dissolving the natural cellulose cotton linter pulp in a low temperature alkali/urea aqueous system, and the cellulose hydrogel was obtained by further introduction of a crosslinker *via* the 'sol–gel' strategy. During this process, the strong hydrogen bond interactions within and between the molecular chains of cellulose were destroyed and recombined, and physical and chemical double crosslinking occurred in the case of the crosslinking agent of epichlorohydrin, resulting in a dense and reticular porous cellulose hydrogel. Furthermore, $Fe(NO_3)_3 \cdot 9H_2O$ was loaded onto the cellulose hydrogel using an impregnation method and followed by repeated washing to obtain the cellulose/Fe composite hydrogel.

ICP-OES was conducted to verify the presence of the Fe species on the cellulose hydrogel. The results indicated that the Fe loading was 1.3%, confirming the successful loading of Fe. FT-IR analysis showed that the characteristic peaks of the initial cellulose gel at 3428, 2921, 1437, 1378, 1046 and 895 cm^{-1} corresponded to the tensile vibration of O–H, the tensile vibration of C–H, the band vibration of C–H, the deformation vibration of C–H and the stretching vibration of the glycosidic bond C–O–C, respectively (Fig. 1a).[28–30] By adding a small amount of EPI, the O–H vibrational peak was slightly shifted, while the other characteristic peaks remained unchanged. This observation was attributed to the crosslinking of EPI with the hydroxyl groups (–OH) along the cellulose chain. After incorporation of iron (Fe), the characteristic peaks of the cellulose/Fe gel attributed to cellulose were also discernible, indicating that the introduction of Fe would not compromise the integrity of the cellulose's structural framework. In the XRD patterns of the initial cellulose gel, cellulose gel and cellulose/Fe gel, the peaks at 12.0°, 19.8° and 21.9° corresponded to the (101), (101) and (002) diffraction planes of the cellulose crystals (Fig. 1b), respectively. However, no characteristic diffraction peaks

belonging to Fe were observed in the cellulose/Fe gel sample. This is likely due to the lower loading or higher dispersion of Fe. XPS spectra in Fig. 1c further confirmed the Fe incorporation, showing that the cellulose/Fe gel consisted of C, O, and Fe elements. Moreover, the Fe 2p spectrum in Fig. 1f displays the binding energy peaks of Fe with different core energy levels. The binding energies of 724.1 eV and 710.7 eV were attributed to the $2p_{1/2}$ and $2p_{3/2}$ of Fe, respectively, with fitting peaks at 713.2 eV belonging to Fe $2p_{3/2}$, indicating the main state of Fe^{3+} in cellulose/Fe gel.[31] Furthermore, the interaction between cellulose and Fe was analyzed by XPS, and the spectrum was calibrated by C 1s at 284.80 eV. By using samples of cellulose gel and cellulose/Fe gel as the example, as shown in Fig. 1d, the binding energy peaks of C 1s in the cellulose gel were mainly concentrated at 284.80, 286.5 and 287.94 eV, corresponding to the sp^2-C/sp^3-C, C–O and C=O bonds, respectively.[32] After loading Fe, the binding energy peaks of C 1s in C–Fe gel were basically unchanged, suggesting that there was no interaction between C and Fe. However, the binding energy peaks of O 1s in the C–Fe gel increased from 532.70 eV to 532.85 eV after loading Fe (Fig. 1e), which may arise from the electron transfer from the lone pair of O atoms to Fe, resulting in a decrease in the electron cloud density of O atoms and an increase in the binding energy.[33] The above results indicated that the Fe species had been successfully incorporated into the cellulose hydrogel, and there was Fe–O coordination interaction between Fe and cellulose.

Furthermore, the microstructure of the cellulose/Fe hydrogels was observed by SEM, as shown in Fig. 2a–f. There was no significant difference in the internal microstructure (plane or section) of the cellulose hydrogel after adding a crosslinking agent or loading Fe. All cellulose-based hydrogels exhibited interconnected porous network structures, and this porous network structure had the following advantages:[34] (1) while
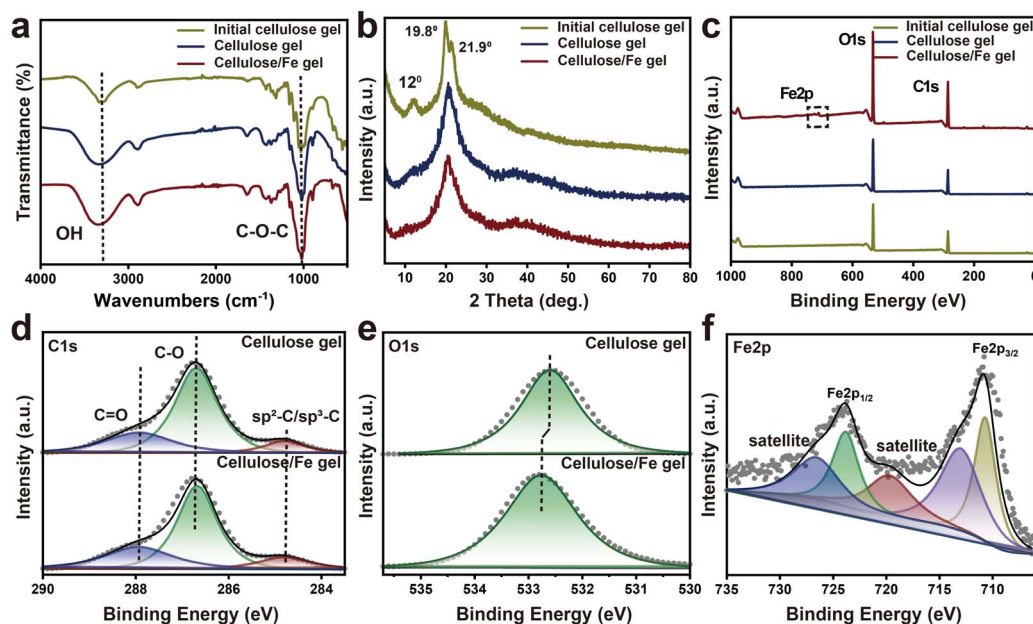
Fig. 1 FT-IR spectra of the initial cellulose gel, cellulose gel and cellulose/Fe gel (a). XRD patterns of the initial cellulose gel, cellulose gel and cellulose/Fe gel (b). Full-scale XPS spectra of the initial cellulose gel, cellulose gel and cellulose/Fe gel (c). C 1s spectrum of the cellulose gel and cellulose/Fe gel (d), O 1s spectrum (e) and Fe 2p spectrum of the cellulose/Fe gel (f).

serving as a microbial barrier, it was beneficial to the diffusion of water-based fluids in the polymer network, increased the swelling capacity of the hydrogel, and accelerated the absorption of exudate or blood; (2) it would help to promote the diffusion and exchange of gas and nutrients at the wound site, making it a good candidate for wound healing materials. The plane and section structures of the cellulose/Fe gel were denser than that of the initial cellulose gel and cellulose gel, which may be due to the introduction of Fe further promoting the coordination crosslinking of cellulose. In the nitrogen adsorption–desorption isotherms (Fig. 2g), all the initial cellulose gel, cellulose gel and cellulose/Fe gel samples showed a hysteresis loop of IV H3 type, indicating that there were a large number of mesopores in the hydrogel materials. In the pore size distribution, the pores in the initial cellulose gel, cellulose gel and cellulose/Fe gel materials were distributed in the range of 2–93 nm, and mainly concentrated in the range of 29–33 nm, further confirming the existence of a large number of mesopores. In the calculated BET surface area, the specific surface area of the cellulose hydrogel with the added crosslinking agent increased from 241.93 $m^2 g^{-1}$ to 313.07 $m^2 g^{-1}$ compared to the initial cellulose gel, which may arise from the formation of extra pores and complex structures in the material. Upon the incorporation of iron (Fe), there was a reduction in the specific surface area compared to the cellulose gel, dropping from 313.07 $m^2 g^{-1}$ to 273.08 $m^2 g^{-1}$. This decrease suggested that the newly formed pore structures within the cellulose matrix were partially obstructed by the introduced Fe particles.

As a wound dressing, the hydrogel also needed to have a certain amount of toughness and stability, so thermogravimetric (TG) analysis and mechanical tensile tests were conducted. TG curves of the initial cellulose gel, cellulose gel and

cellulose/Fe gel are shown in Fig. 2h. Herein, it can be seen that the 5% weight loss temperatures ($T_{5\%}$) of the initial cellulose gel, cellulose gel and cellulose/Fe gel were 273 °C, 273 °C and 263 °C, respectively. When Fe was added to the cellulose hydrogel material, the residual amount at 800 °C increased, indicating that Fe can improve the thermal stability of the cellulose hydrogel. This may be due to the early degradation in the cellulose/Fe gel, forming a protective carbon layer that reduced heat and mass transfer during combustion.[32] These results demonstrated that the cellulose/Fe gel had high thermal decomposition and good thermal stability, making it suitable for use as a wound dressing. In the mechanical tensile test, the stress–strain curves of the initial cellulose gel, cellulose gel and cellulose/Fe gel are shown in Fig. 2i. It can be seen that the tensile strength and fracture strain of the initial cellulose gel were 0.102 MPa and 4.013%, respectively. After the introduction of the crosslinker, the tensile strength and fracture strain of the cellulose gel were 0.82 MPa and 4.329%, respectively. Furthermore, after the introduction of Fe, the mechanical properties of the cellulose/Fe hydrogel improved with the tensile strength and fracture strain increasing to 1.26 MPa and 5.257%, respectively. This enhancement was likely due to the coordination between Fe and cellulose through Fe–O bonds, which led to further cross-linking of the cellulose, thereby improving its mechanical properties. Based on the above results, we selected the samples of the cellulose gel and cellulose/Fe gel for subsequent biomedical experiments.

3.2 ROS scavenging and oxygen generation

H_2O_2 is an active oxide that is ubiquitous in the body, and is produced by the mutation of superoxide ions or the action of
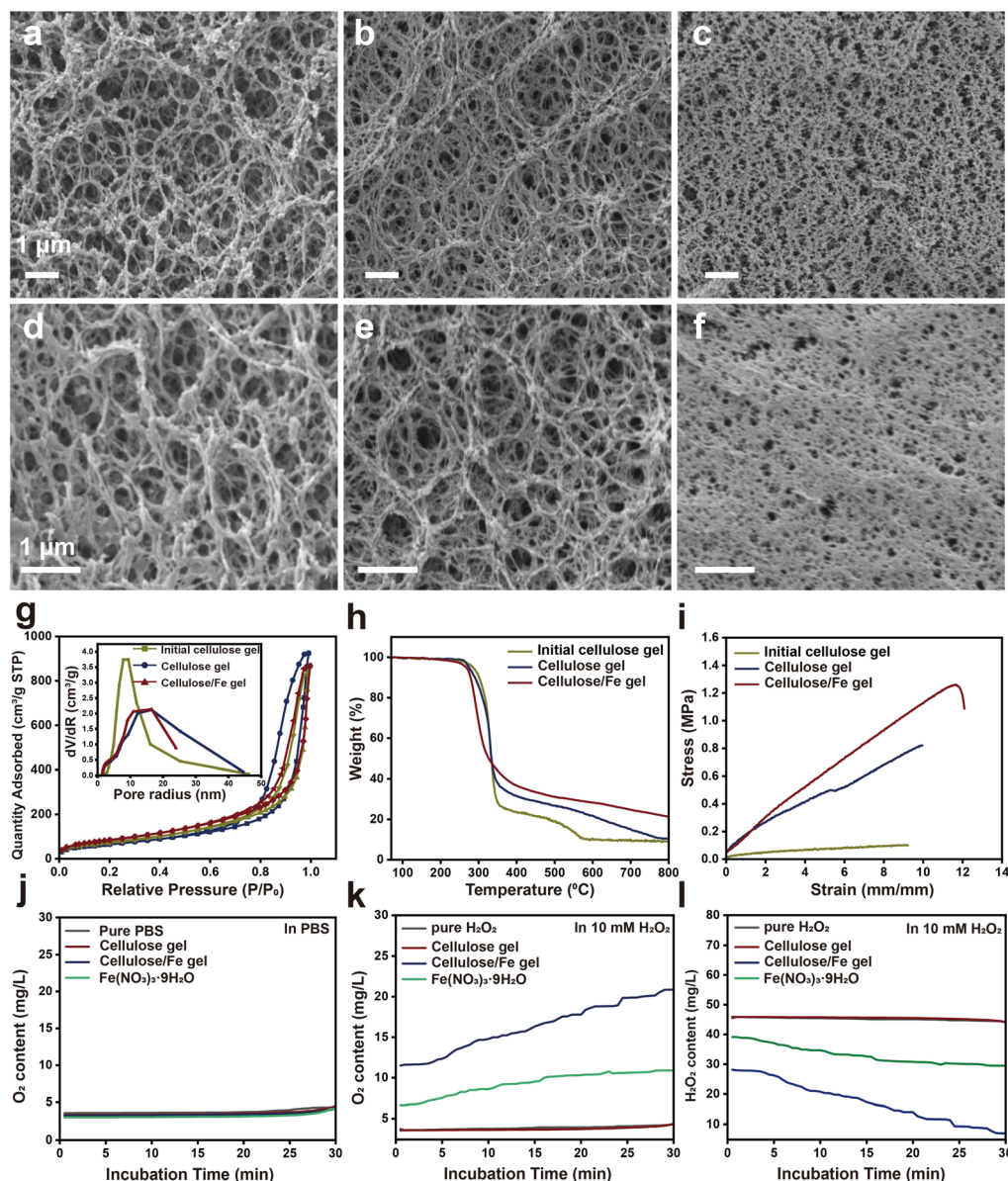
Fig. 2 SEM images of the plane and section of the initial cellulose gel, respectively (a and c). SEM images of the plane and section of the cellulose gel, respectively (b and e). SEM images of the plane and section of the cellulose/Fe gel, respectively (c and f); the scale bar is 1 μm for all images. Illustration of the nitrogen adsorption and desorption isotherms of the initial cellulose gel, cellulose gel and cellulose/Fe gel (g), with the inset showing the pore size distribution. TG diagrams of the initial cellulose gel, cellulose gel and cellulose/Fe gel (h). Tensile stress−strain curves of the initial cellulose gel, cellulose gel and cellulose/Fe gel (i). The amount of O_2 produced over time with PBS (pH = 7.4, 0.01 M) (j) and 10 mM H_2O_2 (k) in the presence of the cellulose gel, cellulose/Fe gel and $Fe(NO_3)_3 \cdot 9H_2O$, respectively. The H_2O_2 content over time in 10 mM H_2O_2 (l).
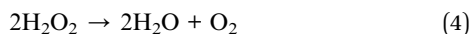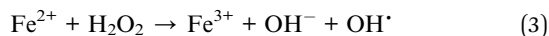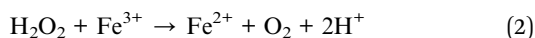
certain oxidase, and can be eliminated by a variety of enzymatic or non-enzymatic systems. The biological effects of H_2O_2 *in vivo* are dose-dependent.[35] Under normal physiological conditions, the low concentration of H_2O_2 (1–10 μM) exhibited suppressed reactivity and limited toxicity to cells. It acted as a chemical attractant for neutrophils, stimulating the proliferation of vascular endothelial cells and fibroblasts. However, a high concentration of H_2O_2 ($\geq$50 μM) will produce strong oxidative stress on the wound tissue and exhibits cytotoxicity to cells. The Fe species can act as a catalyst to promote the decomposition of H_2O_2 and generate oxygen. In addition, H_2O_2 can be converted into some antioxidants through the iron-induced Fenton reaction to form O_2 and H_2O (the reaction formula is as follows: (2)–(4)); thus, it plays a crucial role in inhibiting cellular oxidative stress.[19] As shown in Fig. 2j, the content of O_2 generated by each group of samples in the PBS solution is about 4 mg L^{-1}, without any significant difference. However, in 10 mM H_2O_2 solution, compared with the pure cellulose gel, the content of H_2O_2 in the cellulose/Fe gel was significantly reduced (Fig. 2l), and the content of generated O_2 is greatly increased (Fig. 2k). We believe that the three-dimensional porous structure of the cellulose hydrogel is more conducive to the gas

exchange between these generated O_2 and the surrounding wound, while the removal of H_2O_2 could prevent oxidative stress in the wound and reduce inflammation.

$$H_2O_2 + Fe^{3+} \rightarrow Fe^{2+} + O_2 + 2H^+ \qquad (2)$$

$$Fe^{2+} + H_2O_2 \rightarrow Fe^{3+} + OH^- + OH^· \qquad (3)$$

$$2H_2O_2 \rightarrow 2H_2O + O_2 \qquad (4)$$

3.3 Cytotoxicity evaluation *in vitro*

To evaluate the cytotoxicity of the synthesized cellulose/Fe composite hydrogel *in vitro*, live/dead staining analysis was conducted, and the samples of the Fe salt and cellulose gel were used as controls. As shown in Fig. 3a, the green fluorescent cells represent healthy cells, while the apoptotic cells appear red, which indicates that almost no apoptotic cells were observed in all samples.[36] The results of the MTT method (Fig. 3c) showed that the four groups of comparative experiments did not show obvious cytotoxicity. These results showed that the Fe salt, cellulose gel, and cellulose/Fe gel had good biocompatibility. In addition, we used flow cytometry to further verify the above results and used the mature probe Annexin V/PI to detect apoptotic cells.[37,38] The results showed that the percentage of viable cells in the Fe salt, cellulose gel, and cellulose/Fe gel treatment groups was very similar to that in the blank control group, and there was no significant statistical difference (Fig. 3b–d). It can be seen that the cellulose hydrogel has excellent biocompatibility, which makes the cellulose/Fe gel a potential candidate for biomaterial applications.
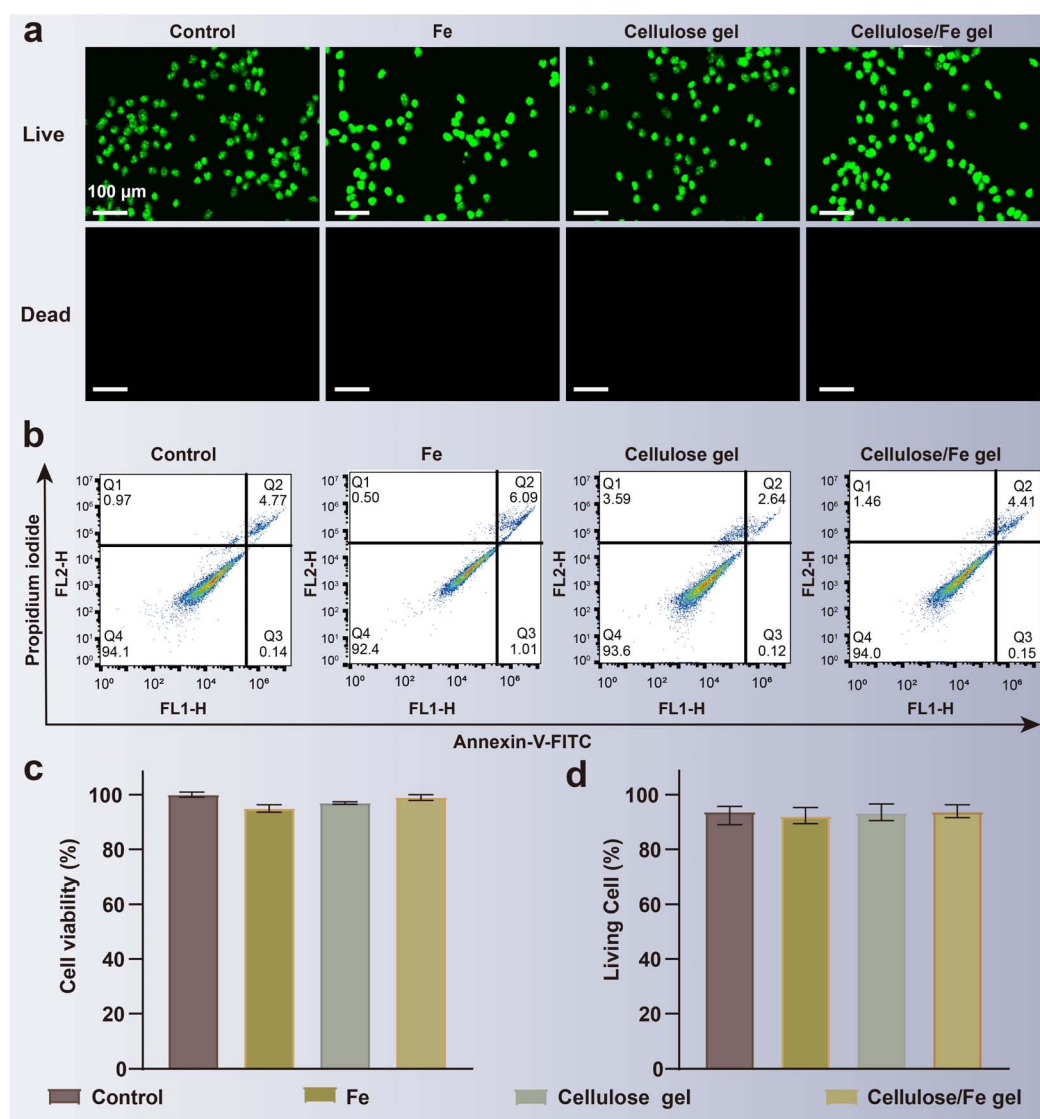
Fig. 3 Live/dead staining was performed on human dermal fibroblasts cells treated with the blank control, Fe salt solution, cellulose gel and cellulose/Fe gel (a). The blank control group, Fe group, cellulose gel group and cellulose/Fe group induced apoptosis of RAW 264.7 cells (b), with Q1, Q2, Q3 and Q4 representing necrosis, late apoptosis, early apoptosis and living cells in the population, respectively. Cell viability of the blank control group, Fe group, cellulose gel group and cellulose/Fe group (c). Percentage of living cells in the blank control group, Fe group, cellulose gel group and cellulose/Fe group (d).

3.4 *In vivo* evaluation and mechanistic analysis of the cellulose/Fe gel on wound healing

Next, we used *in vivo* models to detect the recovery effects of the cellulose/Fe gel. The classical rat skin full-thickness defect

model was used, and the cellulose/Fe gel was coated on the wound to evaluate the repair effect.[39] The wound images on different days are shown in Fig. 4a–c. In Fig. 4a, it can be clearly observed that the wound healing rate of the cellulose/Fe gel
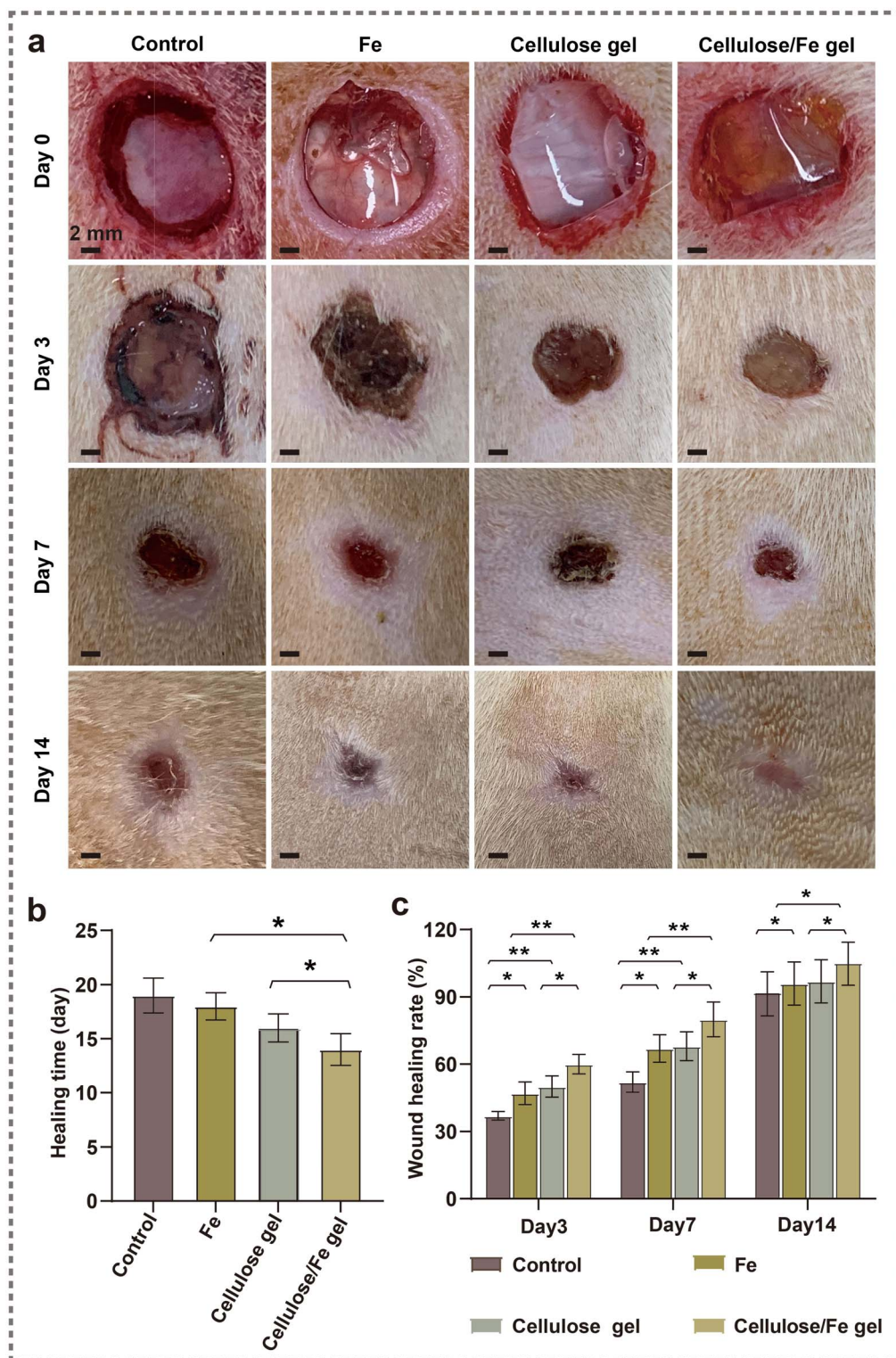

Fig. 4 Photographs of the wound sites treated in the blank control group, Fe salt group, cellulose gel group and cellulose/Fe group on days 0, 3, 7 and 14 (a); with the initial wound diameter being 10 mm; the scale bar is 2 mm. Statistical chart of the healing time (b) and healing rate of the wound (c); ***: $p < 0.001$, **: $p < 0.01$, *: $p < 0.05$.

group reached 60% after only three days of treatment, which was significantly higher than that of the blank control group (37%), Fe group (47%), and cellulose gel group (50%). After 14 days of treatment, as shown in Fig. 4c, the wound closure rates of the above four groups of samples were 88%, 90%, 92%, and 100%, respectively. No open wound was observed in the cellulose/Fe gel group on the 14th day, and the new epidermal tissue was smooth, while the wound area of the other groups still had a rough surface.[40] In summary, the wound healing rate in the sample treated with the cellulose/Fe gel was higher than that of the other groups (Fig. 4b). The best wound healing performance of the cellulose/Fe gel may be attributed to: (1) its three-dimensional porous structure of the cytoplasmic matrix, which can maintain the moist microenvironment around the wound so that a large number of exudates or blood are absorbed, as well as help the exchange of nutrients and the diffusion of oxygen; (2) the introduction of Fe ions can neutralize the negative charge of blood cells, which is conducive to the deposition of colloidal particles to achieve hemostasis and promote the closure of the wound.

To further explore the reason why the cellulose/Fe gel promoted skin wound healing, we examined the collagen deposition and vascular growth in new skin tissues.[41] H&E results showed that the thickness of the granulation tissue in the blank control group, Fe group, cellulose gel group, and cellulose/Fe gel group showed significant differences on the 14th day (Fig. 5a(i)). As shown in Fig. 5b, on the 14th day, the thickness of the granulation tissue at the wound site of the
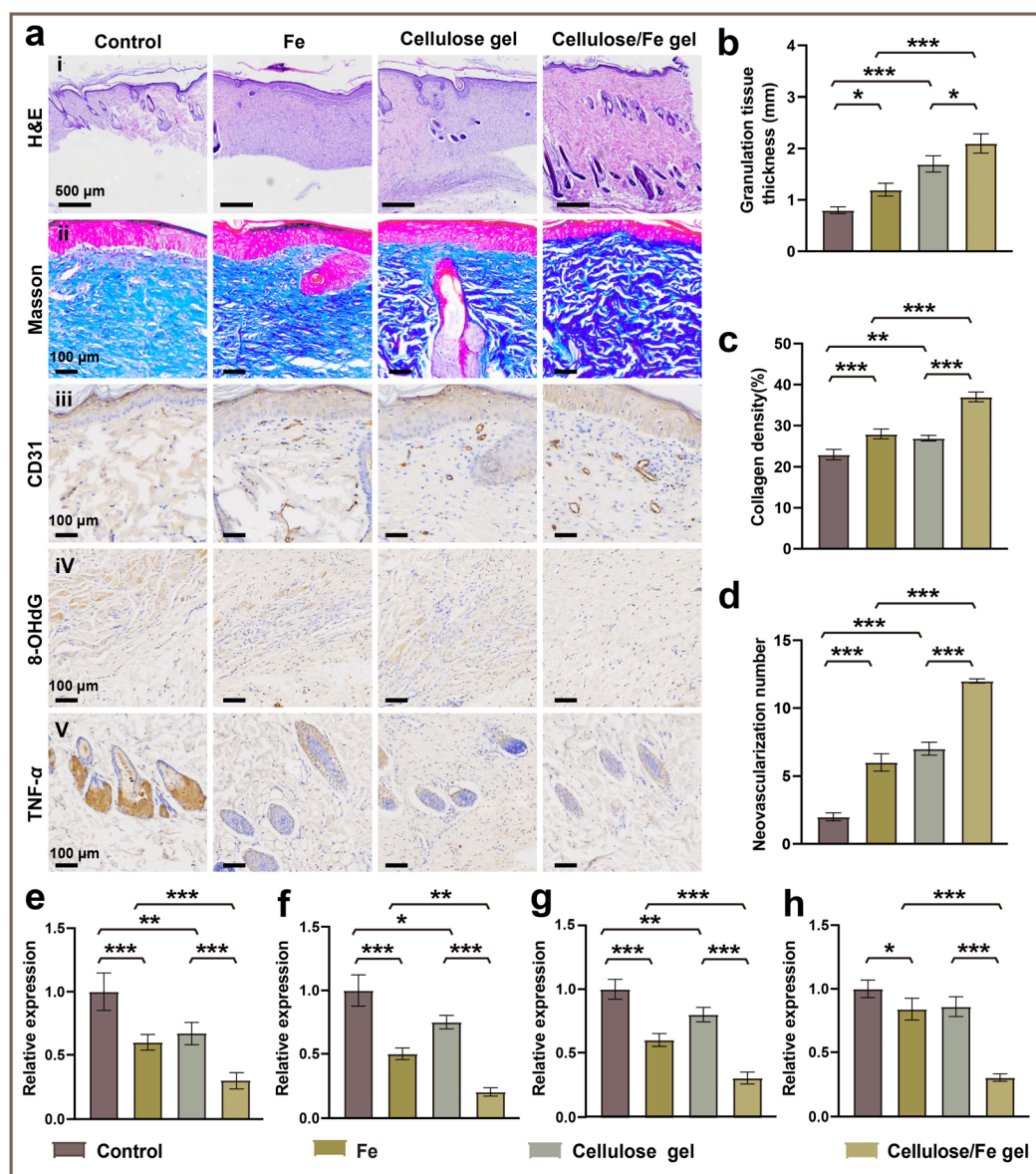

Fig. 5 Microscopic photographs of wound tissues stained (a) with H&E (i), Masson (ii), CD31 (iii), 8-OHdG (iv) and TNF-α (v) on the 14th day (from left to right: blank control group, Fe group, cellulose gel group and cellulose/Fe group). Quantitative analysis of granulation tissue thickness (b), collagen density (c), number of new blood vessels (d), relative expression of 8-OHdG (e), relative expression of TNF-α (f), relative expression of IL-6 (g), and relative expression of IL-1β (h); ***: $p < 0.001$, **: $p < 0.01$, *: $p < 0.05$.

cellulose/Fe gel group was 2.1 mm, which was much higher than that of the blank control group (0.8 mm), the Fe group (1.2 mm), and the cellulose gel group (1.7 mm), indicating that the cellulose/Fe gel group can more readily promote the repair of skin wounds than the other groups. In addition, we used Masson's trichrome staining to evaluate the results of collagen deposition under the wound.[42] Fig. 5a(ii) and statistical analysis results in Fig. 5c showed that the collagen fibers in the blank control group, Fe group, and cellulose/Fe gel group were less expressed and there was partial dysplasia, while the relative expression of collagen in the cellulose/Fe gel group was higher than that in other groups, indicating that the cellulose/Fe gel group had more fibroblasts and collagen formation. Next, we used CD31 (a vessel endothelial cell marker) immunohistochemical staining to analyze the neovascularization (Fig. 5a(iii) and (d)), which indicated that the expression of CD31 in the cellulose/Fe gel group was significantly higher than that in the other groups on the 14th day, indicating that the cellulose/Fe gel can significantly promote neovascularization.[43] These data revealed the reason why the cellulose/Fe gel can significantly promote the wound healing.

To further reveal the mechanism of how the cellulose/Fe gel can significantly promote wound healing, oxidative factors and inflammatory factors were characterized. Usually, 8-hydroxy-2′-deoxyguanosine (8-OHdG) is a marker of oxidative DNA damage in wound tissue.[44] It can be seen that the level of 8-OHdG detected in the cellulose/Fe gel treated wounds was lower than

other control groups (Fig. 5a(iv) and (e)), indicating that the cellulose/Fe gel inhibited the release of oxidative factors. Furthermore, we examined three inflammatory factors of the NF-κB pathway, namely TNF-α, IL-6, and IL-1β.[45] Compared with the other three groups, the cellulose/Fe gel showed lower levels of TNF-α, IL-6, and IL-1β. This indicated that the cellulose/Fe gel had the lowest expression of inflammatory factors (Fig. 5f–h). These data indicated that the cellulose/Fe gel lowered the oxidative factors and inflammatory factors, which could effectively inhibit the inflammatory response in the wound, improve the microenvironment of skin growth, and accelerate the wound healing process. We believe that the Fenton effect caused by the introduction of Fe particles in the cellulose hydrogel can effectively remove some reactive oxygen species and reduce the oxidation factor, as well as effectively prevent oxidative stress in the wound, reduce the inflammatory factors and decrease the occurrence of inflammation. At the same time, the following advantages of the cellulose/Fe gel are summarized as follows: (1) excellent water absorption and moisture retention; (2) good mechanical stability; (3) a three-dimensional porous structure that can accelerate nutrient penetration and oxygen exchange; (4) unique biocompatibility. These features of the cellulose/Fe gel significantly promoted the formation of granulation tissue and epithelization in the cellulose/Fe gel, thereby accelerating the wound healing process. Finally, we evaluated the potential toxicological effects of the cellulose/Fe gel. H&E staining was conducted in the lung, heart, kidney
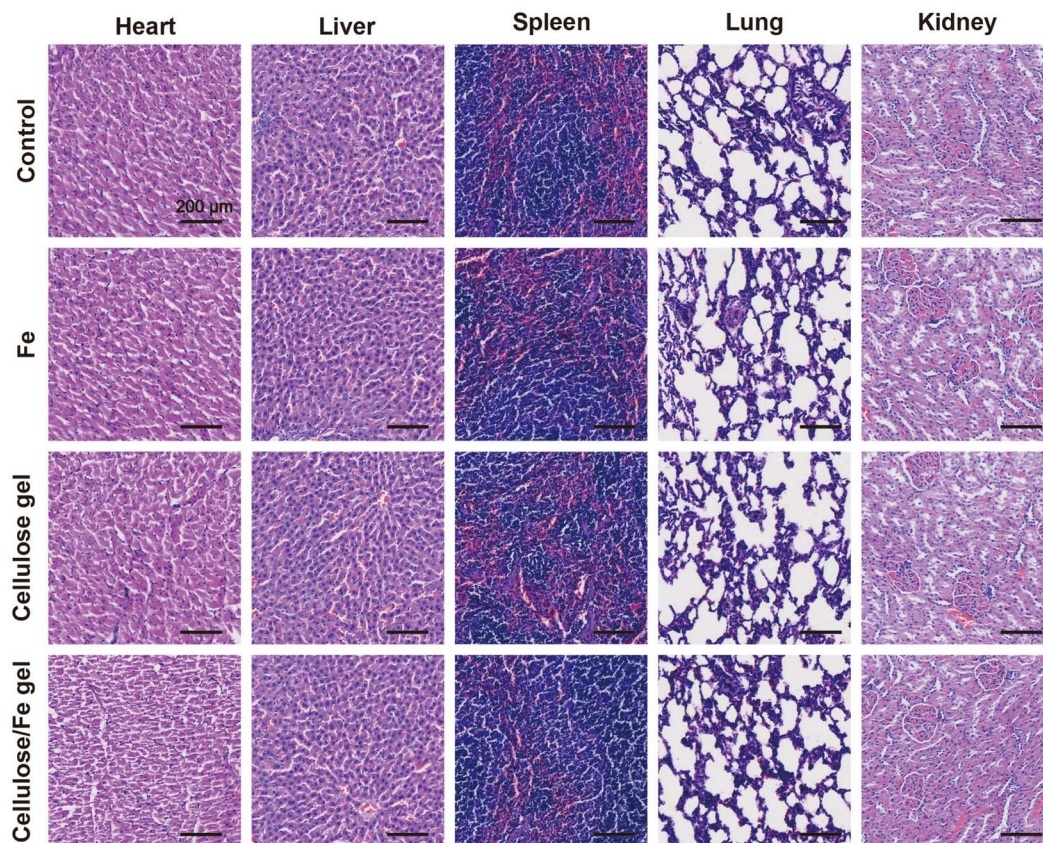

Fig. 6 H&E staining of the main organs after 14 days for various samples.

and live tissues. As shown in Fig. 6, almost no pathological changes were observed in these four groups. The results showed that there were no obvious toxicological effects to the key organs in each group. Thus, it is demonstrated again that the cellulose/Fe gel hydrogel has good biocompatibility and is an ideal wound repair material.

4. Conclusion

In summary, we developed a three-dimensional network cellulose/Fe gel with low cost, strong stability, high biocompatibility, pro-angiogenesis, anti-inflammatory and other beneficial functions. The excellent mechanical properties enable the hydrogel to provide sufficient support as a wound dressing material, and the three-dimensional porous structure facilitates the diffusion and exchange of nutrients and gases. The incorporated Fe has a certain flocculation and hemostasis effect, and can effectively remove reactive oxygen species and inhibit cell oxidative stress, thereby inhibiting the inflammatory response. *In vitro* cytotoxicity evaluation experiments showed that the cellulose/Fe gel had good biocompatibility. The results from the *in vivo* experiments on full-thickness skin wounds in rats showed that the cellulose/Fe gel can effectively promote angiogenesis and collagen matrix secretion, reduce the expression of oxidative factors and inflammatory factors, and significantly promote wound healing. The cellulose/Fe gel is characterized as a 'green' material with high biocompatibility and low cytotoxicity. It significantly promotes wound repair, and has great potential as multifunctional wound dressing materials for clinical applications.

Data availability

The authors confirm that the data supporting the findings of this study are available within the article.

Author contributions

Mingyue Xue: conceptualization, writing – review & editing, visualization, formal analysis, investigation, data curation. Jian Zhang, Cuiling Niu and Hongqin Wang: formal analysis, investigation, data curation. Xianglin Pei, Ling Nie and Jiuyang Ding: conceptualization, writing – review & editing, visualization, formal analysis, investigation, data curation.

Conflicts of interest

The authors have no conflicts of interest to declare with respect to the research, authorship and publication of this article.

Acknowledgements

References

1 R. Gu, H. Zhou, Z. Zhang, Y. Lv, Y. Pan, Q. Li, C. Shi, Y. Wang and L. Wei, *Nanoscale Adv.*, 2023, **5**, 6017–6037.

2 Y. Gao, M. Ikeda-Imafuku, Z. Zhao, M. Joshi and S. Mitragotri, *Bioeng. Transl. Med.*, 2023, **8**, 10516.

3 Y. Wang, K. Liu, W. Wei and H. Dai, *Adv. Funct. Mater.*, 2024, **34**, 2402531.

4 D. Huang, J. Du, F. Luo, G. He, M. Zou, Y. Wang, Z. Lin, D. Wu and Z. Weng, *Adv. Healthcare Mater.*, 2024, **13**, 2303379.

5 A. Arin, M. S. Rahaman, U. Farwa, J. Gwon, S. H. Bae, Y. K. Kim and B. T. Lee, *Int. J. Biol. Macromol.*, 2024, **262**, 130094.

6 N. Tang, R. Zhang, Y. Zheng, J. Wang, M. Khatib, X. Jiang, C. Zhou, R. Omar, W. Saliba, W. Wu, M. Yuan, D. Cui and H. Haick, *Adv. Mater.*, 2022, **34**, 2106842.

7 H. M. Nguyen, T. T. Ngoc Le, A. T. Nguyen, H. N. Thien Le and T. T. Pham, *RSC Adv.*, 2023, **13**, 5509–5528.

8 F. J. Shariatzadeh, S. Currie, S. Logsetty, R. Spiwak and S. Liu, *Prog. Mater. Sci.*, 2025, **147**, 101350.

9 A. Haider, S. Khan, D. N. Iqbal, S. U. Khan, S. Haider, K. Mohammad, G. Mustfa, M. Rizwan and A. Haider, *Int. J. Biol. Macromol.*, 2024, **278**, 134172.

10 L. Tian, T. Liu, Y. Jiang, B. He and H. Hao, *Chem. Eng. J.*, 2024, **497**, 154890.

11 X. Zhang, Y. Liang, S. Huang and B. Guo, *Adv. Colloid Interface Sci.*, 2024, **332**, 103267.

12 X. Fu, Y. Chen, G. Hu, J. Lv, J. Liu, M. Ma and X. Fu, *Int. J. Biol. Macromol.*, 2023, **332**, 127116.

13 Y. Chen, Y. Zhang, L. Chang, W. Sun, W. Duan and J. Qin, *Int. J. Biol. Macromol.*, 2023, **246**, 125644.

14 C. Ma, L. Du, Y. Guo and X. Yang, *Int. J. Biol. Macromol.*, 2024, **280**, 135838.

15 H. Cheng, Q. Yu, Q. Chen, L. Feng, W. Zhao and C. Zhao, *Biomater. Sci.*, 2023, **11**, 931–948.

16 Y. Ai, Z. Lin, W. Zhao, M. Cui, W. Qi, R. Huang and R. Su, *J. Mater. Chem. B*, 2023, **11**, 7004–7023.

17 Q. Qin, S. Zeng, G. Duan, Y. Liu, X. Han, R. Yu, Y. Huang, C. Zhang, J. Han and S. Jiang, *Chem. Soc. Rev.*, 2024, **53**, 9306–9343.

18 G. Zhang, C. Yu, Y. Dong, W. Su, R. Xue, P. Zhang, Y. Li, G. Wan, K. Tang and X. Fan, *Biomater. Adv.*, 2025, **166**, 214025.

19 X. Guo, D. Xu, Y. Zhao, H. Gao, X. Shi, J. Cai, H. Deng, Y. Chen and Y. Du, *ACS Appl. Mater. Interfaces*, 2019, **11**, 34766–34776.

20 Y. Iwasaki, Y. Ookuro, K. Iida, K. Nagasawa and W. Yoshida, *Biochem. Biophys. Res. Commun.*, 2022, **15**, 134–139.

21 Y. Zhang, J. Huang, M. Sun, Y. Duan, L. Wang, N. Yu, D. Peng, W. Chen and Y. Wang, *Heliyon*, 2023, **9**, e12819.

22 K. J. Lee, K. P. Ulrich N'deh, G. J. Kim, J. W. Choi, J. Kim, E. K. Kim and J. H. An, *ACS Appl. Bio Mater.*, 2021, **4**, 1252–1267.

23 Y. Li, W. Xiu, K. Yang, Q. Wen, L. Yuwen, Z. Luo, X. Liu, D. Yang, X. Xie and L. Wang, *Mater. Horiz.*, 2021, **8**, 1264–1271.

24 C. Tu, H. Lu, T. Zhou, W. Zhang, L. Deng, W. Cao, Z. Yang, Z. Wang, X. Wu, J. Ding, F. Xu and C. Gao, *Biomaterials*, 2022, **286**, 121597.

25 M. Stindlova, V. Peroutka, V. Jencova, K. Havlickova and S. Lencova, *J. Microbiol. Methods*, 2024, **224**, 107010.

26 M. Ding, Y. Yang, Z. Zhang, H. Liu, Y. Dai, Z. Wang, S. Ma, Y. Liu and Q. Wang, *Int. J. Biol. Macromol.*, 2024, **268**, 131891.

27 L. Zhang, Y. Wang, M. Yang, W. Yu, Z. Zhao and Y. Liu, *Polymers*, 2024, **16**, 1316.

28 Y. Guo, X. Wang, Y. Shen, K. Dong, L. Shen and A. A. A. Alzalab, *J. Mater. Sci.*, 2022, **57**, 58–104.

29 M. Naeimirad, B. Krins and G. J. M. Gruter, *Sustainability*, 2023, **15**, 14474.

30 F. Lyu, S. Zeng, Z. Jia, F. X. Ma, L. Sun, L. Cheng, J. Pan, Y. Bao, Z. Mao, Y. Bu, Y. Li and J. Lu, *Nat. Commun.*, 2022, **13**, 6249.

31 K. S. Bejigo, R. S. A. Saravanan, K. Bhunia and S. J. Kim, *Green Chem.*, 2024, **26**, 6100–6108.

32 C. Zhou, J. Wang, K. Wu, Z. Pan, Q. Cheng, L. Feng, H. Wu and H. Zhou, *ACS Sustainable Chem. Eng.*, 2022, **10**, 13453–13464.

33 A. A. Adesibikan, S. S. Emmanuel, C. O. Olawoyin and P. Ndungu, *J. Organomet. Chem.*, 2024, **1010**, 123087.

34 S. M. Hwang, E. Kim, J. Wu, M. H. Kim, H. Lee and W. H. Park, *Int. J. Biol. Macromol.*, 2024, **277**, 134098.

35 W. Wang, W. Jiang, G. Mao, M. Tan, J. Fei, Y. Li and C. Li, *Anal. Chem.*, 2021, **93**, 3301–3307.

36 J. Ouyang, A. Xie, J. Zhou, R. Liu, L. Wang, H. Liu, N. Kong and W. Tao, *Chem. Soc. Rev.*, 2022, **51**, 4996–5041.

37 T. Chen, F. Xing and Y. Sun, *J. Exp. Nanosci.*, 2024, **19**, 2281938.

38 J. P. Robinson, R. Ostafe, S. N. Iyengar, B. Rajwa and R. Fischer, *Cells*, 2023, **12**, 1875.

39 J. Cao, P. Wu, Q. Cheng, C. He, Y. Chen and J. Zhou, *ACS Appl. Mater. Interfaces*, 2021, **13**, 24095–24105.

40 M. U. A. Khan, M. A. Aslam, T. Yasin, M. F. B. Abdullah, G. M. Stojanović, H. M. Siddiqui and A. Hasan, *Biomed. Mater.*, 2024, **19**, 052001.

41 M. Nichifor, *Polymers*, 2023, **15**, 1065.

42 W. Zhang, X. Li, W. Chen, X. Huang, T. Hua, J. Hu, J. Zhu, S. Ye and X. Li, *RSC Adv.*, 2024, **14**, 18317–18329.

43 Y. Wu, Z. Yang, X. Li, T. Li, J. Zheng, M. Hu, Z. Yu, W. Luo, W. Zhang, F. Zheng, T. Tang and Y. Wang, *Chem. Eng. J.*, 2023, **477**, 147145.

44 A. Buczyńska, M. Kościuszko, I. Sidorkiewicz, A. A. Wiatr, A. Adamska, K. Siewko, J. Dzięcioł, M. Szelachowska, A. J. Krętowski and A. Popławska-Kita, *J. Clin. Endocrinol. Metab.*, 2024, **109**, 1866–1872.

45 J. Liu, T. Wang, C. Liao, W. Geng, J. Yang, S. Ma, W. Tian, L. Liao and C. Cheng, *Adv. Mater.*, 2024, **36**, 2411618.